

Sponsored by—  
American Institute of Aeronautics and Astronautics (AIAA)  
Society of Automotive Engineers (SAE)

**AIAA PAPER**  
**No. 75-1212**

INLET PERFORMANCE OF THE INTEGRATED LANGLEY SCRAMJET  
MODULE (MACH 2.3 TO 7.6)

by  
CARL A. TREXLER  
NASA Langley Research Center  
Hampton, Virginia

AIAA PAPER 75-1212

**AIAA/SAE 11th**  
**Propulsion Conference**

ANAHEIM, CALIFORNIA/SEPTEMBER 29-OCTOBER 1, 1975

For permission to copy or republish, contact the American Institute of Aeronautics and Astronautics,  
1290 Avenue of the Americas, New York, N.Y. 10019.

M75-16576

INLET PERFORMANCE OF THE INTEGRATED LANGLEY SCRAMJET MODULE

(MACH 2.3 TO 7.6)

Carl A. Trexler  
 NASA Langley Research Center  
 Hampton, Virginia 23665

Abstract

The inlet concept for the Langley Scramjet Module has been developed and proven in Langley wind tunnels over a Mach number range from 2.3 to 6.0 (flight simulation of Mach 2.6 to 7.6). This modular engine concept is designed to integrate with the airframe, which results in precompression of the engine airflow by the vehicle bow shock and additional expansion of the nozzle exhaust gas by the afterbody of the vehicle. With these integration advantages, the inlet can be designed with modest contraction ratios and fixed geometry. Also, the module nozzle exit area can be equal to the capture area, which permits the cowl to be aligned with the local flow producing minimum external drag. The inlet leading edges and planar compression surfaces are swept at 48°, which provides spillage at low Mach numbers for starting and which reduces the pressure gradient on the top surface to permit ingestion of the vehicle forebody boundary layer into the inlet without separating. Three fuel injection struts provide for the use of a short combustor having low internal cooling requirements. Schedules for mass capture ratio, contraction ratio, and total pressure recovery are well within the acceptable range for a good scramjet propulsion device. The fixed geometry, minimum external drag design has proven to be a practical, high-performance inlet concept.

Nomenclature

$A_1$	Area of captured stream tube at inlet face
$A_c$	Inlet frontal area, 290 cm <sup>2</sup>
$A_T$	Area of captured stream tube at inlet throat
$A_1/A_c$	Inlet capture
$A_1/A_T$	Aerodynamic contraction ratio, $\frac{A_1}{A_T} \left( \frac{A_T^*}{A_T} \right) (P_{t,T}/P_{t,1})$ where $A_T/A_T^* = f$ (mass average Mach number at throat)
$C$	Distance downstream from cowl leading edge
$H$	Inlet height, 19.05 cm
$M$	Mach number
$P$	Static pressure
$P_{t,T}/P_{t,1}$	Mass average total pressure recovery
$Y$	Perpendicular distance from model foreplate

$X$	Distance downstream of foreplate leading edge
$X_2$	Distance downstream of sidewall leading edge
$X_3$	Distance downstream of strut leading edge
$A$	Sweep angle, deg
$\eta_k$	Kinetic energy efficiency
<u>Subscripts</u>	
$\infty$	Vehicle flight conditions
$1$	Conditions behind vehicle body shock or at inlet face
$T$	Conditions at inlet throat
$t$	Total property

Introduction

The attractive potential of hypersonic flight with airbreathing propulsion has been recognized and firmly established by a number of successful research-scale engine demonstrations in the 1960's.<sup>1-3</sup> These research and development programs for hypersonic airbreathing engines have generated a broad technology base and have demonstrated engine concepts with practical levels of thrust.<sup>4</sup> However, major advances in technology are still required, and the NASA Langley Research Center is actively engaged in a research and technology program to define and develop a viable airbreathing propulsion system for hypersonic flight applications. The first application will probably be in a small research airplane to demonstrate performance under flight conditions (Fig. 1). The leading candidate for this system is the supersonic combustion ramjet (scramjet) engine shown in Figure 2 which illustrates the next logical step in scramjet evolution, the integration of the engine with the airframe. Integration includes the use of the vehicle forebody to precompress the engine airflow before it enters the inlet and the use of the vehicle afterbody for additional expansion and thrust vectoring of the nozzle exhaust gas. Other principal design criteria for hypersonic systems are minimum engine cooling requirements to make part of the heat sink of the hydrogen fuel available for active cooling of the airframe, fixed geometry to reduce weight and system complexity, and minimum external drag.

Currently, research work is focused on an in-house-conceived, hydrogen-burning, airframe-integratable, engine module (Langley Scram Module, shown in Figure 3 and discussed in Ref. 5), and intensive theoretical, analytical, and experimental efforts are underway toward the practical definition of the engine module's basic components, such as the

inlet, combustor, and nozzle, as well as toward the practical integration of the basic components. With vehicle-engine integration advantages, the module nozzle exit area can be equal to the inlet capture area which permits the cowl to be aligned with the local flow producing minimum external drag. This paper deals with the design and performance evaluation of the inlet portion of the engine module. Again, vehicle-engine integration permits the inlet to be designed with a modest contraction ratio and fixed geometry. Low internal cooling requirements primarily result from the short combustor design made possible by the use of three fuel injection struts, which also contribute to the inlet flow compression.

#### Experimental Program

Several design iterations have resulted in the inlet configuration of Figure 3, and additional design philosophy concerning sweep angle, contraction, height-to-width ratio, and inlet starting can be found in Reference 6, which describes the results of testing the inlet at a local Mach number of 6.0 (summarized in Ref. 7). The inlet model shown in Figure 4 had a projected geometric capture area measuring 19.05 cm high by 15.24 cm wide, resulting in a projected, rectangular capture area of 290 cm<sup>2</sup>. The leading edges of the sidewall compression surfaces and all downstream stations were swept at 48° to provide spillage at low Mach numbers for starting. Spillage would occur through the open window upstream of the cowl leading edge, which is bathed by shocks produced by the sidewalls. Nominal compression surface angles of 6° (measured in a plane parallel to the foreplate) reduced the risk of boundary-layer separation from incident and reflecting shock waves generated by the sidewalls and struts. The sidewalls and struts were also relieved in areas of shock-wave concentrations at high Mach number conditions. The combination of the sweep angle, the sidewall design, and the cowl leading-edge location were selected to produce near-maximum mass capture ratios as a function of Mach number. Boundary layer generated on the vehicle forebody was expected to be ingested by the inlet safely because the swept shock system reduces the pressure gradients on the topwall. The model was 90.2 cm long, not including the 46-cm foreplate. This foreplate had large boundary-layer trips near the leading edge to provide a thick boundary layer entering the inlet, which partially simulated the boundary layer on the forebody of a hypersonic vehicle.

The model was heavily instrumented as described in Reference 6 to obtain both wall and survey pressure measurements for a detailed performance evaluation. Pitot and static pressure rakes surveyed the throats of the model to obtain total pressure recovery and Mach number, and a constant area section downstream of the struts was also surveyed to determine the inlet capture.

The aerodynamic performance over the entire operational Mach number range of the air-induction system (the inlet) is an important factor in establishing the viability of an airbreathing, supersonic/hypersonic engine (scramjet) design. The Langley Scram inlet test program had proven the successful operation of the inlet in the Langley 20-Inch Tunnel at a Mach number of 6 (Reynolds number =  $9.8 \times 10^6$  per meter and  $3.3 \times 10^6$  per meter)

at the face of the inlet. This represents a flight Mach number of approximately 7.6 when 8° of two-dimensional flow turning is attributed to the vehicle body shock. However, in order to complete the inlet test program, the fixed geometry inlet had to be proven at lower Mach numbers and several objectives were set.

(1) First to determine if the inlet would start at a Mach number at least as low as 3.0, which is the lower boundary of the proposed operating range.

(2) To determine the inlet capture schedule, because inlet operation at low Mach numbers requires large amounts of spillage.

(3) To determine the inlet contraction, recovery, and throat Mach number to verify that they are adequate for successful engine performance.

(4) To insure that the swept 3-D shock waves do not pose a problem as they move along the sidewalls and struts.

Therefore, to obtain these objectives, the model was tested in the high Mach number leg of the Unitary Plan Wind Tunnel, which has a Mach number range of 2.3 to 4.6. When coupled with the Mach 6 tests; the tested flight Mach number range is 2.6 to 7.6. The unit Reynolds number for the 2.3 to 4.6 tests was  $6.6 \times 10^6$  per meter ( $2.0 \times 10^6$  per foot).

#### Discussion of Results

##### Shock-Wave Systems

The computed shock-wave systems for the inlet are shown in Figure 5 for the Mach numbers tested and illustrate what was expected to occur in these tests. A computer program utilizing a normal component method to calculate an inviscid, swept-shock-wave train can be found in Reference 6. The diagrams are in a plane parallel to the cowl and no end effects from the top surface or cowl are considered. At the lower Mach numbers, the shock waves become detached before the inlet throats are reached, as indicated by the letter D. These detached shock waves are curved and provide the additional spillage necessary for supersonic low Mach number operation without inlet choking. The shock waves become attached at the inlet throat at about Mach 5. For the current configuration, at a Mach number of about 4.5, the reflected sidewall shock wave combines with the side strut shock wave at the side strut leading edge. For an earlier configuration, this characteristic occurred at Mach 6; the combined shock waves provided too much contraction and partial choking resulted near the cowl. At the lower Mach numbers with the current design, the detached shock waves were expected to prevent this condition.

Schlieren photographs for local Mach numbers of 2.3 and 4.6 are given in Figure 6. Because the swept shock waves are skewed relative to the plane of the schlieren, interpretation of the results is difficult. The shock waves on the top of the model are the result of the support apparatus which reduces the major regions of interest to the Mach waves extending from the leading edge of the foreplate and to the shock waves at the bottom of the model in front of the cowl. A large number of "detached" shock waves extend from the bottom of the

model for the Mach 2.3 test condition, which is synonymous with large amounts of spillage. At a Mach number of 4.6, most of the waves are absent and the most noticeable characteristic is the steep wave located slightly ahead of the cowl leading edge. As the flow passes through the swept shock waves, it is turned away from the top surface and toward the cowl, creating a local increase in contraction. The schlierens indicate subsonic flow may exist next to the cowl during low Mach number operation of the inlet, even though the shock waves may be computed to be attached at the leading edges of the struts. The effect of this small subsonic flow region on the combustor and engine performance is yet to be evaluated; although no pictures were available, static pressure data indicated that this condition did not exist for the Mach 6 test.

#### Static-Pressure Distributions

Static-pressure distributions are provided in Figures 7-14 for the top surface, cowl, struts, and sidewalls of the inlet. Three of the Mach number tests ( $M_1 = 6.0, 4.6, \text{ and } 2.3$ ) are compared and represent various stages of inlet operation. Each pressure has been nondimensionalized by the tunnel static pressure in front of the model. The expected low static pressure near the top surface (Fig. 7) is realized because the swept compression surfaces turned the flow away from this region. These low pressures permitted the boundary layer generated on the foreplate to enter the inlet, and should likewise allow the boundary layer on the forebody of a hypersonic vehicle to pass through the inlet without separating. Concurrently, the static pressure near the cowl (Fig. 8) is high due to the flow being turned into this region. The Mach 2.3 tests show a decrease in static pressure indicating subsonic flow next to the cowl. For a Mach number of 4.6 the pressure associated with the strong shock wave is present, particularly in the center passage. For the Mach 6 tests, the pressure level continues to rise along the cowl surface as would be expected for supersonic flow.

The static-pressure data measured for the center passage at  $Y/H = 0.43$  and  $0.88$  and at the throat (Figs. 9, 10, and 11) were obtained from orifices located on the side strut. For a Mach number of 2.3, the detached shock waves and a large amount of spillage greatly reduced the amount of inlet compression. Near the center of the inlet ( $Y/H = 0.43$ ) the static pressure increase for  $M_1 = 4.6$  and  $6.0$  is well behaved, while the effects of the increased cowl pressures at  $Y/H = 0.88$  are evident for  $M_1 = 4.6$ . This cowl pressure extends up about 20% of the strut as shown in Figure 11. Three-dimensional end effects as a function of Mach number are clearly seen in Figure 11. For  $M_1 = 6.0$  the low-pressure region near the top surface extends down the strut until  $Y/H = 0.4$ . The value of  $Y/H$  increases to about 0.5 for  $M_1 = 4.6$ , and this effect is enhanced by the detached shock waves for  $M_1 = 2.3$  and extends the entire length of the strut. The up-and-down pattern of static pressure along the center passage throat for  $M_1 = 6.0$  is also attributed to end effects where a shock wave generated by the fillet on the top surface slightly moves the concentrated swept shock-wave system near the row of static-pressure orifices which are located at the minimum area of the center passage.

Except for  $M_1 = 2.3$  the maximum pressure levels in the side passage (Figs. 12, 13, and 14) are approximately one-half of those of the center passage. The rise in static pressure at  $M_1 = 6.0$  downstream of the side passage throat (Fig. 13) is due to the shock wave from the cowl striking the sidewall downstream of the expansion fan created by the break in the side strut at the throat. The static-pressure orifices for the side passage throat (Fig. 14) were located on the strut 0.30 cm ahead of the break on the strut. The smaller number of shock waves and lower pressures in the side passage reduces the appearance of three-dimensional effects from the top surface, even though they may still exist.

#### Throat Mach Number and Total Pressure Recovery

Surveys of a center passage and a side passage throat were made with a pitot probe at five different stations along the struts. Also, a specially designed, short, static probe<sup>8</sup> surveyed a center passage throat, which left the side passage static-pressure distribution to be obtained from wall values at the throat. The survey data were processed and analyzed by a digital computer program which by a curve-fitting interpolation procedure expanded the data into a network of approximately 1000 grid points, covering the entire throat flow area. Besides performing numerical integrations, Mach number, total pressure, and unit mass flow were calculated for each grid point; and contour maps of each parameter were plotted by the computer's graphics system.

The resulting Mach number contours and total pressure recoveries are given in Figures 15-20 for the  $M_1$  conditions of 6.0, 4.6, and 2.3. The width of each passage is shown six times its unswept height to better distinguish the contour lines; however, this distortion tends to exaggerate the significance of the corners when related to the total flow area. Most of the vertical walls were relieved near the cowl surface to partially counteract the excess compression produced by the cowl shock; however, the scale differences also exaggerate this relief on the figures. For both passages, there was some rounding of the flow contours at the corners, with the boundary layers being thicker on the sidewall and top surfaces than on the struts, but no flow separation was detected. The discrete shock wave generated by the cowl is smeared by the interpolation process producing the appearance of a thick boundary layer near the cowl for  $M_1 = 6.0$  and 4.6.

The side passage Mach number contours are relatively symmetrical, unlike the center passage because of the greater number of shock waves in this passage. Very slight shifts in the position of the swept shock waves alter the survey data at the throat station as well as magnify the error associated with determining the exact position of the survey probes. However, the mass weighted average Mach number contour for the center passage encloses the major portion of the total flow area. The  $M_1 = 2.3$  contours indicate that supersonic flow did exist at the throat with the average throat Mach number being 1.28. The Mach number for  $M_1 = 2.3$  reached a value of 1.4 for the side passage and 1.6 for center passage. The subsonic portion is, for the most part, in the top surface boundary layer and represents about 18%

of the flow for the two passages. This area was largest at this low Mach number because the boundary-layer flow filled the void area created by the large amount of spillage. From the static-pressure distributions along the cowl (Fig. 8) for low Mach number operation, it is suspected that the flow becomes subsonic next to the cowl and then returns supersonic at the swept throat. The effect of this characteristic on combustor operation is as yet undetermined, but it does have a stabilizing effect on the inlet.

#### Integrated Performance

Mass weighted averages are given in Figures 21-24 for four integrated parameters significant to engine cycle performance. For the throat Mach number and contraction curves, the circles are for the side passage and the squares for the center passage. The solid lines and the circles on the capture and total pressure recovery curves are mass averaged with approximately two-thirds of the captured flow passing through the two center passages. This flow split was determined analytically to be a small function of Mach number and depends primarily on the location of the side strut leading edges.

The predicted capture on Figure 21 was determined by two-dimensionally matching flow direction and pressure behind the shock waves in front of the cowl and neglecting viscous and three-dimensional end effects. Additive drag associated with the spillage of the inlet at low Mach numbers may be significantly important and will have to be determined experimentally because of the difficulty in analyzing the spilled three-dimensional flow. The large amount of spillage at the low Mach numbers (38% capture at  $M_1 = 2.3$ ), combined with the varying aerodynamic contraction (Fig. 22), enabled the inlet to be started at very low Mach numbers. The throat Mach number data (Fig. 23) indicate starting and operation to values of  $M_1$  probably below 2.0. This wide operating range is unique for a hypersonic inlet. The inlet recovery (Fig. 24) is shown to be 85% at Mach 3 and 60% at Mach 6, which was quite good. Corresponding values of kinetic energy efficiency are also shown on the figure.

#### Concluding Remarks

The inlet concept for the Langley Scramjet Module has been developed and proven in wind tunnels over a Mach number range from 2.3 to 6.0 (flight simulation of 2.6 to 7.6), as part of a research and technology program focused on the development of a concept for an airframe-integrated scramjet engine. The swept compression surfaces and downstream location of the cowl enabled the hypersonic, fixed geometry inlet to spill flow and start at a low Mach number. Low-pressure gradients near the top of the inlet should permit the boundary layer on the forebody of a hypersonic vehicle to enter the inlet without separating. The three fuel-injection struts shorten the combustor and reduce engine cooling requirements. With vehicle integration, a modest contraction ratio made starting easier, also reduced cooling requirements, and still enabled the inlet to exhibit good performance over the wide Mach number range. Schedules for

mass capture ratio, contraction ratio, and total pressure recovery are either equal to or slightly less than earlier predictions, but well within the acceptable range for a good scramjet propulsion device.

A minimum of external drag has been designed into the inlet with the cowl parallel to the vehicle underbody and the utilization of the vehicle afterbody for additional expansion of the nozzle flow. The additive drag penalty, because of the large amount of spillage at low Mach numbers, must be determined. However, this flow is spilled downward providing a lift increment to the vehicle. Overall, the swept, modular design has proven to be a practical high-performance inlet concept, and provides an excellent baseline for future work in integrated hypersonic inlets.

#### Acknowledgments

The author wishes to express his gratitude to James M. Mueller and to William J. Monta for their helpfulness in conducting the tests and to Sue W. Souders for her continued support in the data reduction phase of the test program.

#### References

- <sup>1</sup>Henry, J. R., and McLellan, C. H., "The Air-Breathing Launch Vehicle for Earth-Orbit Shuttle -- New Technology and Development Approach," AIAA Paper No. 70-269, Feb. 1970, also Journal of Aircraft, Vol. 8, No. 5, May 1971, pp. 381-387.
- <sup>2</sup>Ferri, A., "Review of SCRAMJET Propulsion Technology," Journal of Aircraft, Vol. 5, No. 1, Jan.-Feb. 1968, pp. 3-10.
- <sup>3</sup>Becker, J. V., "New Approaches to Hypersonic Aircraft," Presented at Seventh Congress of International Council of the Aeronautical Sciences, Rome Italy, Sept. 1970, also Astronautics and Aeronautics, Vol. 9, No. 8, Aug. 1971, pp. 32-39.
- <sup>4</sup>Brown, David A., et al., "Development of Liquid-Hydrogen Scramjet Key to Hypersonic Flight," Aviation Week and Space Technology, McGraw-Hill, Sept. 17, 1973, pp. 75-78.
- <sup>5</sup>Henry, J. R., and Anderson, G. Y., "Design Considerations for the Airframe-Integrated Scramjet," Presented at the First International Symposium on Air Breathing Engines, Marseille, France, June 19-23, 1972.
- <sup>6</sup>Trexler, C. A., and Souders, S. W., "Design and Performance at a Local Mach Number of 6 of an Inlet for an Integrated Scramjet Concept," TN D-7944, May 1975, NASA.
- <sup>7</sup>Trexler, C. A., "Performance of an Inlet for an Integrated Scramjet Concept," Journal of Aircraft, Vol. II, No. 9, Sept. 1974, pp. 589-591.
- <sup>8</sup>Pinckney, S. Z., "An Improved Static Probe Design," AIAA Journal, Vol. 12, No. 4, April 1974, pp. 562-564.

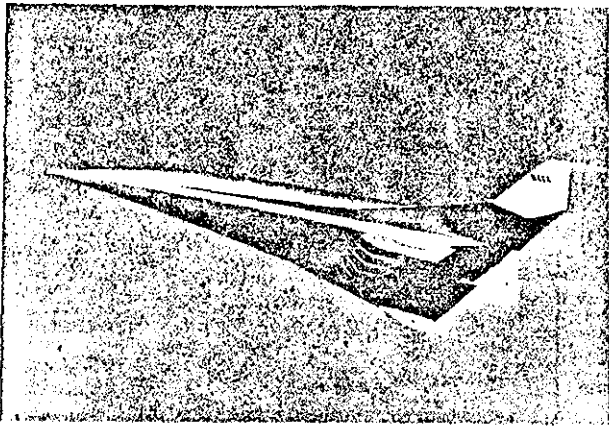


Figure 1. Hypersonic research airplane.

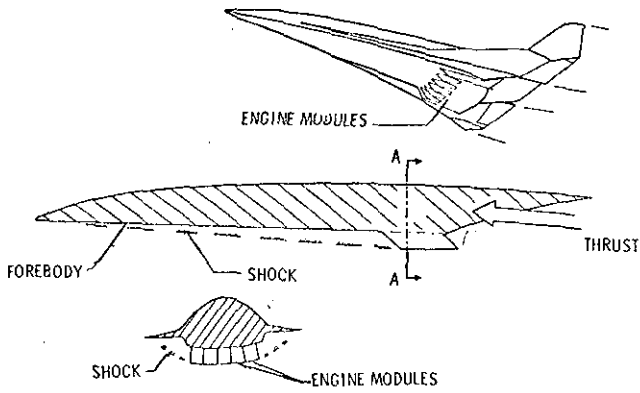


Figure 2. Airframe-scramjet-engine integration.

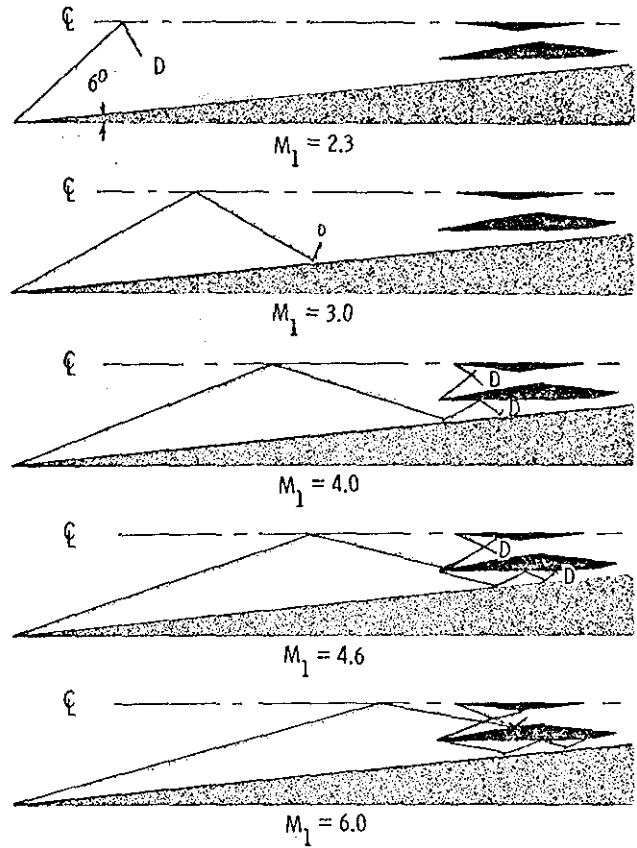


Figure 5. Inlet shock-wave systems, sweep angle =  $48^\circ$ .

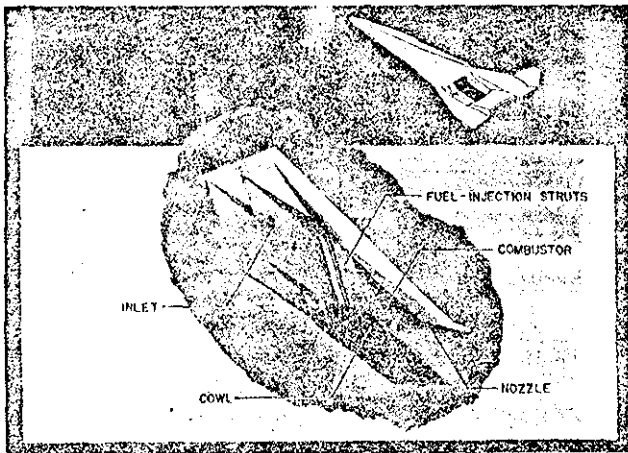
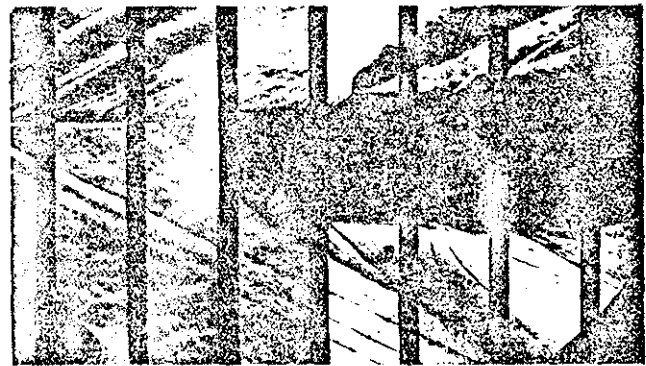
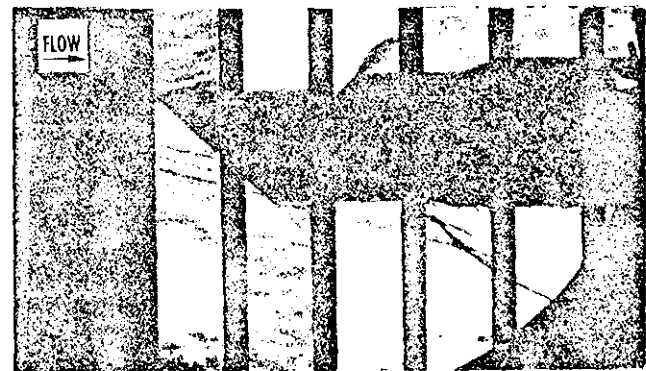


Figure 3. Scramjet modules.



(a)  $M_1 = 2.3$ .



(b)  $M_1 = 4.6$ .

Figure 6. Schlieren photographs of the model in the Langley Unitary Plan wind tunnel.

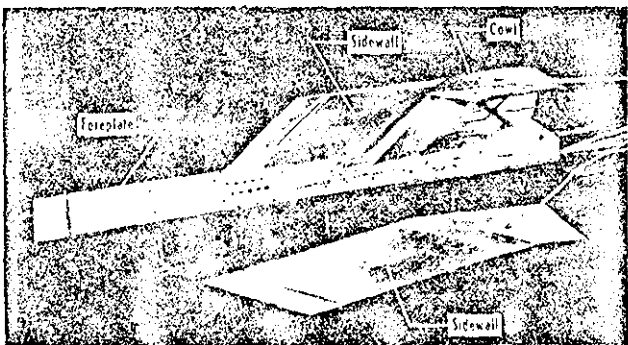


Figure 4. Inlet model.

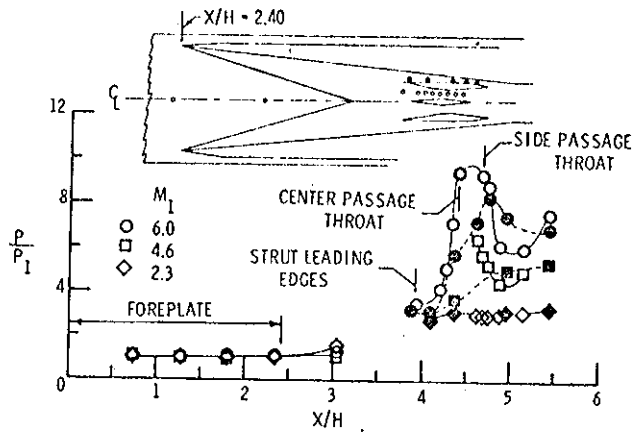


Figure 7. Top surface static pressure.

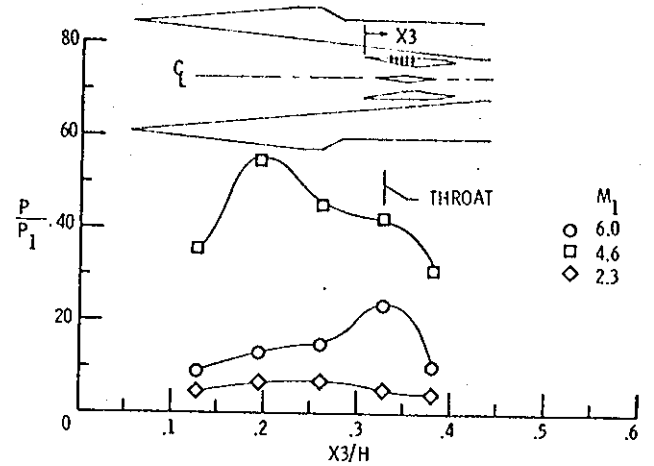


Figure 10. Center passage static pressure ( $Y/H = 0.88$ ).

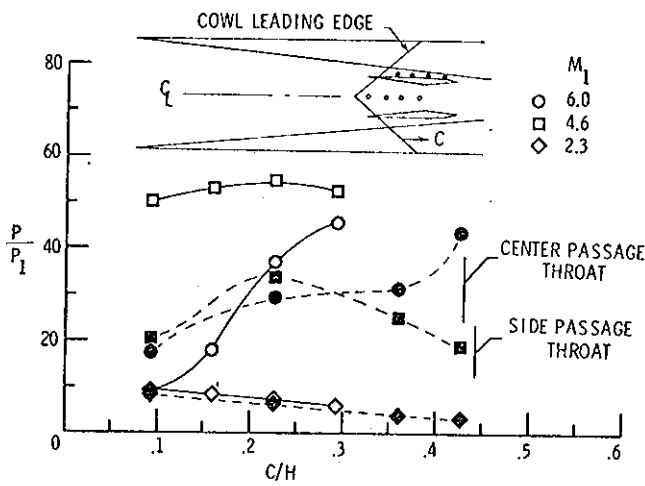


Figure 8. Cowl static pressure.

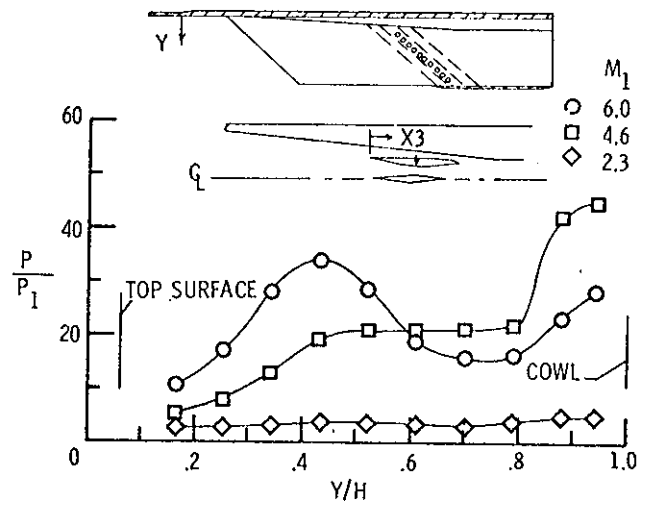


Figure 11. Center passage static pressure ( $X3/H = 0.33$ ).

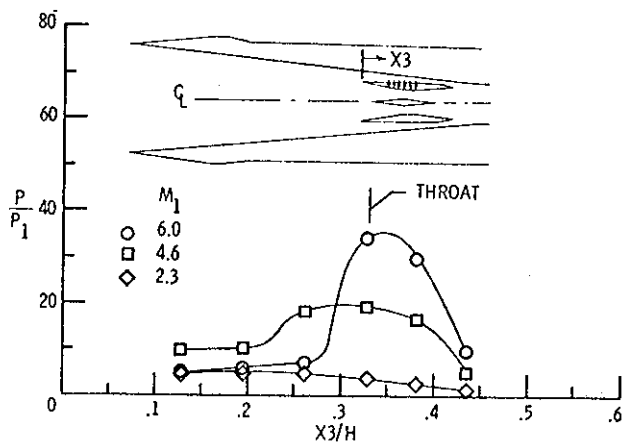


Figure 9. Center passage static pressure ( $Y/H = 0.43$ ).

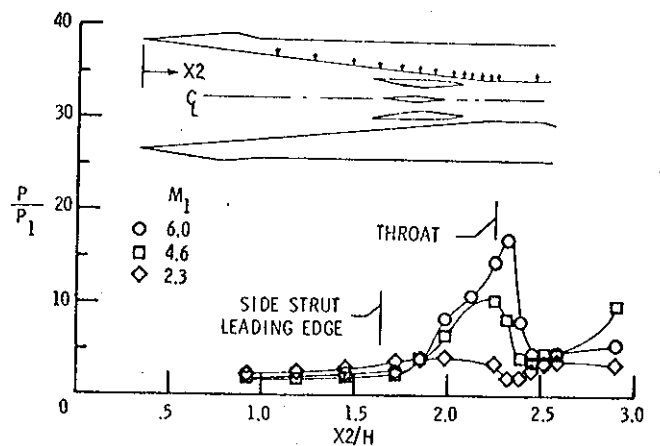


Figure 12. Sidewall static pressure ( $Y/H = 0.43$ ).

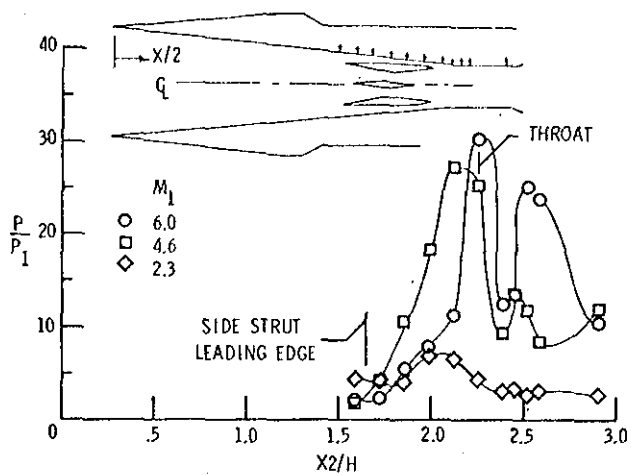


Figure 13. Sidewall static pressure ( $Y/H = 0.88$ ).

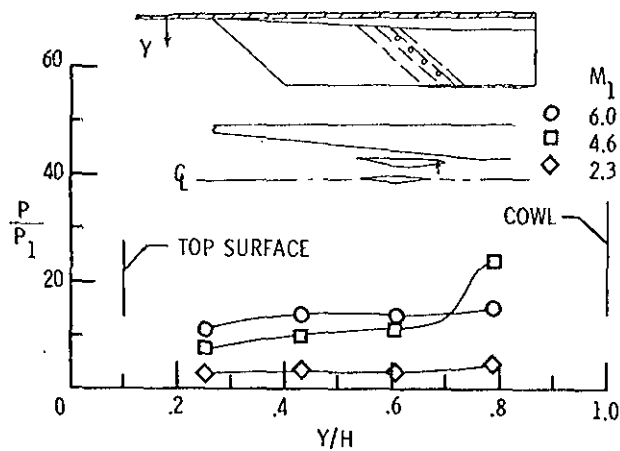


Figure 14. Side passage throat static pressure.

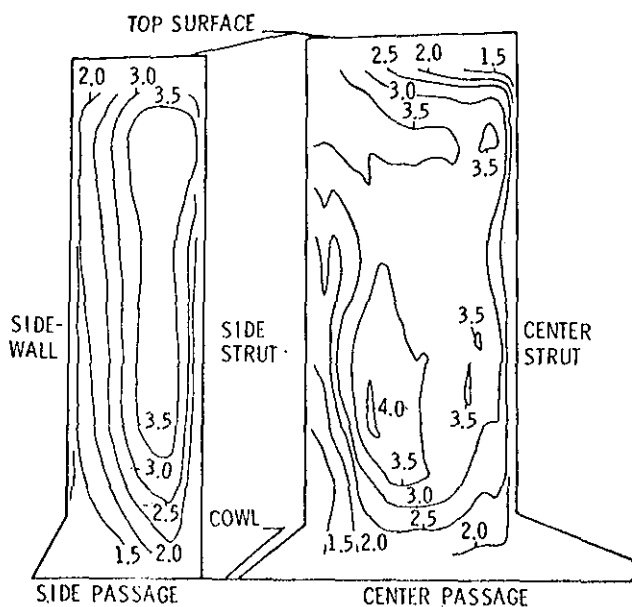


Figure 15. Throat Mach number contours ( $M_1 = 6.0$ ).

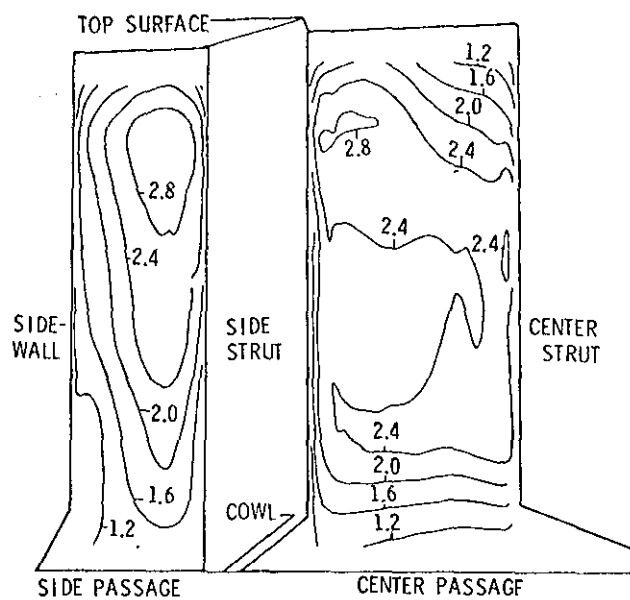


Figure 16. Throat Mach number contours ( $M_1 = 4.6$ ).

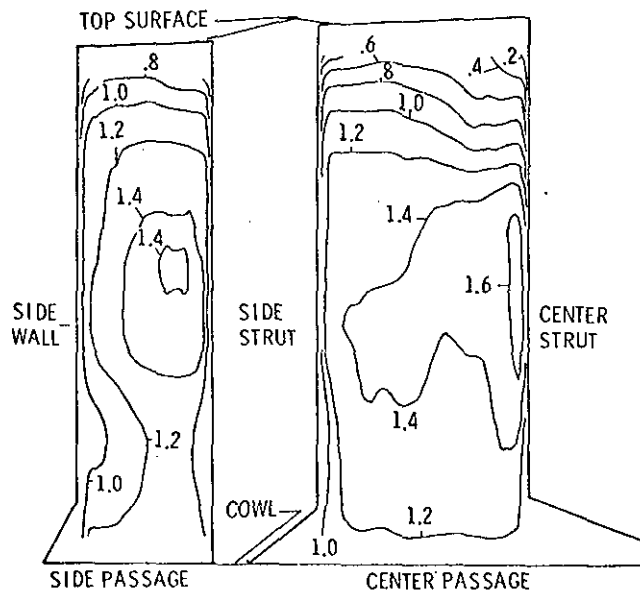


Figure 17. Throat Mach number contours ( $M_1 = 2.3$ ).

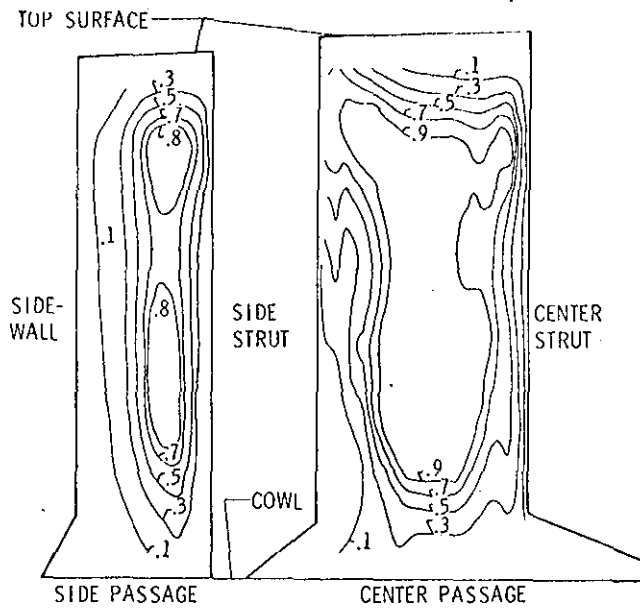


Figure 18. Recovery contours ( $M_1 = 6.0$ ).

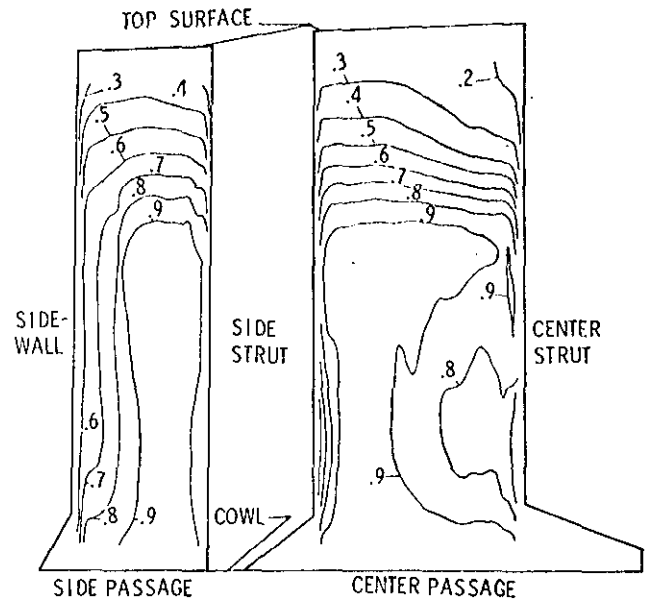


Figure 20. Recovery contours ( $M_1 = 2.3$ ).

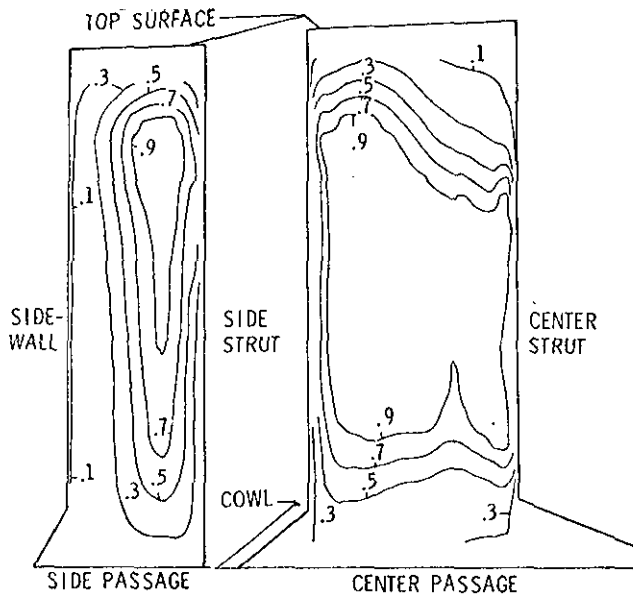


Figure 19. Recovery contours ( $M_1 = 4.6$ ).

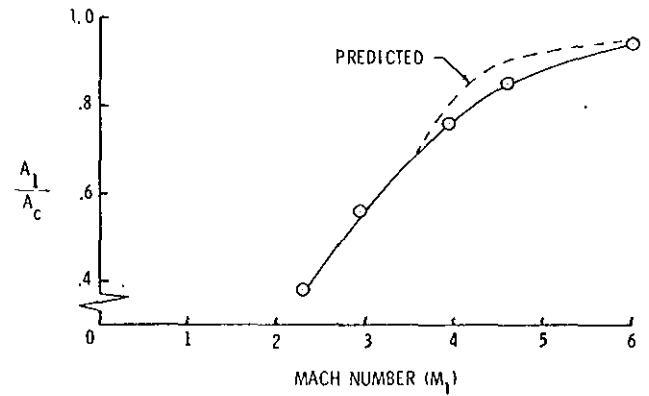


Figure 21. Inlet capture.

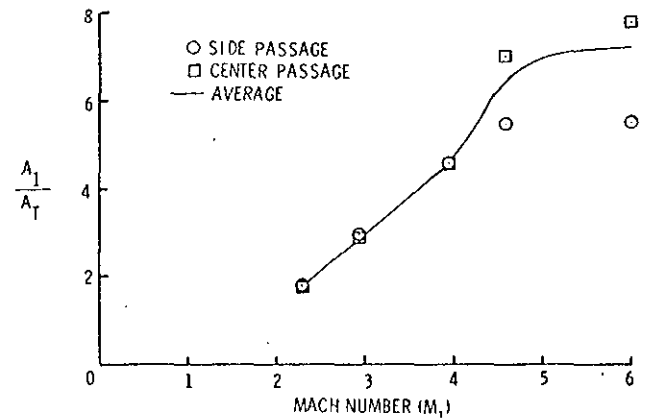


Figure 22. Inlet contraction.

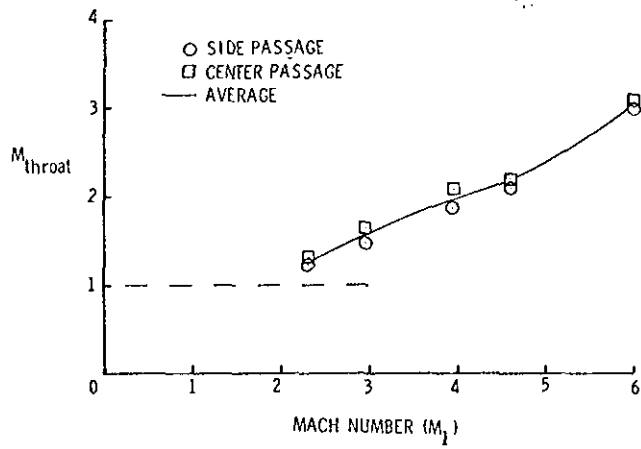


Figure 23. Throat Mach number.

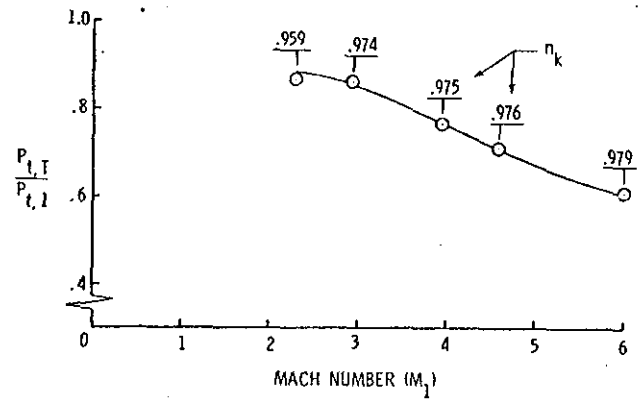


Figure 24. Total pressure recovery.